CARBON 78 (2014) 102–112

Available at www.sciencedirect.com

ScienceDirect

journal homepage: www.elsevier.com/locate/carbon

Graphene–metamaterial hybridization for enhanced terahertz response

Jiayuan Li [a], Yixuan Zhou [a], Baogang Quan [b], Xuecong Pan [b], Xinlong Xu [a,*], Zhaoyu Ren [a,*], Fangrong Hu [c], Haiming Fan [a], Mei Qi [a], Jintao Bai [a], Li Wang [b], Junjie Li [b], Changzhi Gu [b]

[a] State Key Lab Incubation Base of Photoelectric Technology and Functional Materials, International Cooperation Center for National Photoelectric Technology and Functional Materials, and Institute of Photonics & Photon-Technology, Northwest University, Xi'an 710069, China

[b] Beijing National Laboratory for Condensed Matter Physics, and Institute of Physics, Chinese Academy of Sciences, Beijing 100190, China

[c] Electronic Engineering Department, Guilin University of Electronic Technology, Guilin 541004, China

ARTICLE INFO

Article history:
Received 3 March 2014
Accepted 21 June 2014
Available online 28 June 2014

ABSTRACT

Improving the interaction of graphene with terahertz (THz) waves in experiment – through experimental measurement is a challenge for THz detectors, modulators, and other THz photonic components based on graphene. Hybridization of graphene with metamaterials leads to a strong THz response enhancement. Here, we observed maximum enhancement of 33.0% in non-resonant region and 23.8% in resonant region with the hybridization of graphene and metamaterials in experiment. A coupling model as well as numerical calculation has been carried out to fully investigate the influence of this coupling. The results suggest that there exists an exponential relationship between coupling strength and THz response in both resonant and non-resonant region, while the resonant frequency shift shows a linear growth with coupling strength. The bandwidth of the resonance shows exponential increasing with the damping constant. Correspondingly, the numerical calculation shows the similar dependency with the electrical conductivity of the graphene overlayer. This suggests a higher conductivity for stronger coupling. Substrates could also bring the remote phonon scattering, charge transfer, and dielectric effect, which show the influence such as low dielectric constant for high coupling.

1. Introduction

Different with the visible-infrared and microwave region, terahertz (THz) region is regarded as a 'gap' in the electromagnetic spectrum resulting from a lack of efficient devices to manipulate THz wave, but is full of potential applications such as finger-print spectroscopy, biological imaging, high-speed communication. A long search for efficient materials for THz science and technology is a key issue to bridge the 'gap' in THz community [1].

Graphene, two-dimensional carbon atoms in honeycomb lattices, has exhibited remarkable electrical and mechanical properties such as high carrier mobility (200,000 $cm^2\ V^{-1}\ s^{-1}$) [2], flexibility, high mechanical strength, and good stability,

* *Corresponding authors:* Fax: +86 29 88303336.
E-mail addresses: xlxuphy@nwu.edu.cn (X. Xu), rzy@nwu.edu.cn (Z. Ren).
http://dx.doi.org/10.1016/j.carbon.2014.06.053
0008-6223/

which have stimulated extensive attention in recent years [3]. Its optical properties are also fascinating [4] for photonics and optoelectronics. For instance, its quantum constant transparency for each layer in the visible-infrared region [5] and giant broadband nonlinear optical absorption [6], result in promising applications in the next generation of photonic and optoelectronic devices. Unlike the carrier dynamics in the visible-infrared region, which is dominated by the interband transitions, THz carrier dynamics demonstrates intraband transitions in graphene [7,8]. The intraband carriers of graphene in THz region exhibit sensitive, broadband, and ultrafast Drude response [7–10], which are tunable due to the bipolar electric field effect. Significantly, owing to the carrier concentration of pristine graphene on the scale of 10^9–10^{12} cm^{-2}, the plasmon resonance in graphene can reach the THz region [11], which is also tunable by patterning. Based on these THz properties, graphene becomes a promising material for the development of detectors [12,13] and modulators [9,14,15] operating in THz region. However, THz wave has a relatively weak interaction with graphene and the responsivity of the previous graphene-based THz detectors is relatively low. In Vicarelli's work [12], their THz detector based on graphene field-effect transistors structure shows a maximum responsivity of 150 mV per watt, which is quite low compared with other detectors (22.7 kV per watt) [16]. This is mainly due to the limited THz absorption when only pristine graphene is used [4]. The relatively weak THz response of graphene limits its applications in future THz devices.

Metamaterials afford efficient method to design and tailor nature materials for naturally unavailable properties [17] and enhanced optical processes [18,19] owing to their surface plasmon effects. In order to further enhance the optical response of graphene and to extend the photonic applications of graphene, the coupling of graphene and metamaterials has been investigated [18–24]. Significantly, this coupling is quite spectral dependent due to different dynamics of intraband or interband carrier transition of graphene in different spectrum region. Many researches focus on visible-infrared region as the interband carrier coupling with the metamaterials. In Papasimakis's work [20], they show that the graphene–metamaterial interband carrier coupling shows more than 250% variation in the infrared spectral response. Similarly, Zou et al. [22] also proved this efficient interband carrier coupling in the infrared region through numerical simulations. Sarau et al. [18] demonstrated that this graphene–metamaterial coupling can enhance Raman scattering of graphene. Wu et al. [24] proposed a graphene–Au nanoparticle hybrid structure and indicated the presence of multilayer graphene shell imparted significantly low scattering with red-shifted peaks for encapsulated Au nanoparticles in visible region. However, to our best knowledge, there are only few reports on the intraband carrier coupling between graphene and metamaterials in THz region [19,23]. Graphene is suggested for the broadband THz materials but low responsivity and metamaterials are suggested for sensitive THz devices but narrowband responsivity. This intraband carrier coupling could improve the properties of both metamaterials and graphene to achieve win–win characteristics in THz region. Even though Valmorra et al. [19] realized the active control of metamaterials with graphene, more information such as the mechanism of this coupling and the specific contribution of the substrate effects to this coupling are still unclear in THz region.

Nitrogen-doped (N-doped) graphene as another graphene-based material can tune the carrier concentration due to the change of molecular bond properties [25]. In N-doped graphene, the Fermi level shifts above the Dirac point [26] and the density of state near the Fermi level is suppressed [27]. As a result, N-doped graphene shows the *n*-type semiconductor carrier dynamics [28], leading to absolutely different carrier dynamics and carrier coupling with metamaterials compared with the pristine graphene. To the best of our knowledge, the relevant report of the coupling between N-doped graphene and metamaterial has not been available in literatures yet. As the N-doped graphene show mainly electron response (*n*-type doped), this investigation could promote the exploration of electron interaction of N-doped graphene with metamaterials.

In this work, large-area graphene and N-doped graphene synthesized by atmospheric pressure chemical vapor deposition (APCVD) are transferred onto metamaterials. THz time-domain spectroscopy (THz-TDS) is utilized to evaluate the THz response of graphene–metamaterial hybrid structure. The results suggested that the hybridization of graphene (or N-doped graphene) with THz metamaterials can dramatically enhance THz response of both metamaterials and graphene in both non-resonant region (maximum enhancement of 33.0%) and resonant region (maximum 23.8%). THz response of this graphene–metamaterial hybrid structure in non-resonant region can be broadband (0.48 THz in bandwidth) and can be further tuned by metamaterial design. THz resonant response is red-shifted and is sensitive to the micro-environmental dielectrics. To understand this enhancement, both a coupling model and a numerical calculation are employed to reveal the interactions of intraband carrier of graphene with the metamaterials in THz region. The analysis suggests that there exists exponential relationship between coupling strength K_c and THz response in both resonant and non-resonant region, while the resonant frequency shift show a linear growth with coupling strength K_c. The bandwidth of the resonance shows exponential increasing with the damping constant Γ_{add}, which mainly determines the shape of resonance as well as the bandwidth of resonances with a higher damping for broader spectral response. Corresponding to the coupling model, the numerical calculation shows the similar dependency with the electrical conductivity of graphene overlayer. This suggests that a higher conductivity for stronger coupling, which can be achieved by the sample preparation, and the change of this coupling under the modulation of the electrical conductivity always realize via the coupling strength K_c and damping constant Γ_{add}. Meanwhile, substrates could bring the remote phonon scattering, charge transfer, and dielectric effect, which show the influence such as low dielectric constant for high coupling. This intraband carrier coupling in graphene–metamaterial in THz region shows promising applications in THz photodetector and conductivity sensor. Our results further deepen the understanding of intraband carrier in graphene coupled to metamaterials in THz region.

2. Experimental

2.1. Material fabrication

Our metamaterials are fabricated on both Si (800 μm in thickness) and SiO_2 (thickness of 500 μm) substrates in the format of *U*-shaped split ring resonators (SRRs). The structural parameters of SRRs are as follows: the length of a SRR 43 μm, the width 43 μm, the gap 4 μm, width of the line 4 μm, period 55 μm, and the thickness of Au film 80 nm (in Fig. 1). The whole scale of the metamaterials can reach $1 \times 1\ cm^2$. The detailed fabrication process of SRRs is shown in the Supplementary Material.

Large-area graphene and N-doped graphene films were grown on 25 μm Cu foils (Alfa-Aesar, 99.8% purity) by APCVD at temperature up to 1000 °C through the same synthesis process as demonstrated in our previous work [25]. We used CH_4 as the carbon source in graphene synthesis. CH_4 and NH_3, which served as carbon source and nitrogen source respectively, were used to synthesize N-doped graphene. The detailed process is depicted in Supplementary Material. After growth process, Cu foil was dissolved in the etchant ($Fe(NO_3)_3$:HCl:H_2O = 1 g:1 mL:20 mL). Then, graphene and N-doped graphene were directly transferred onto SRRs as demonstrated in Fig. 1. The transfer process of graphene and N-doped graphene onto SRRs was finished by the wet transfer technology with the metamaterial samples fixed in the sample stage and the detailed transfer process is shown in the Supplementary Material.

2.2. Material characterization

X-ray photoelectron spectroscopy (XPS) and Raman spectrometer were used to characterize graphene and N-doped graphene (NG1 and NG2). The XPS spectra of NG1 and NG2

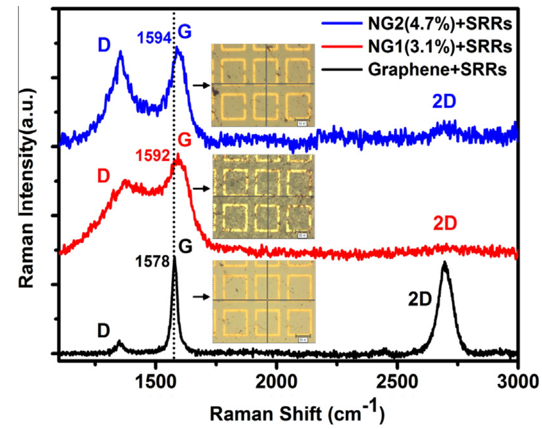

Fig. 2 – Raman spectra of pristine graphene and N-doped graphene with 3.1 (NG1) and 4.7 (NG2) at.% doping concentrations on SRRs array surface. Inset: optical image at the collection-point for Raman spectrum. (A color version of this figure can be viewed online.)

(Figs. S1 and S2 in Supplementary Material) confirm the existence of N atoms in graphene lattice and show the atomic percentage of N atoms in NG1 and NG2 are 3.1% and 4.7% respectively (Sensitivity factor method is employed to calculate the atomic percentage of N [29]). As shown in Fig. 2, the Raman spectrum of the pristine graphene (black curve) demonstrates a small D mode located at 1350 cm^{-1}, a strong and sharp G mode located at 1581 cm^{-1}, and a 2D mode located at 2700 cm^{-1}. The intensity ratio of D and G mode is very small which reveals the pristine graphene is of high quality with few defects [30]. Compared with pristine graphene, N-doped graphene (red curve for 3.1% (NG1) and blue curve for 4.7% (NG2) doping concentrations) has a stronger D mode, a broader G mode, a strong blue-shifted G mode, and a

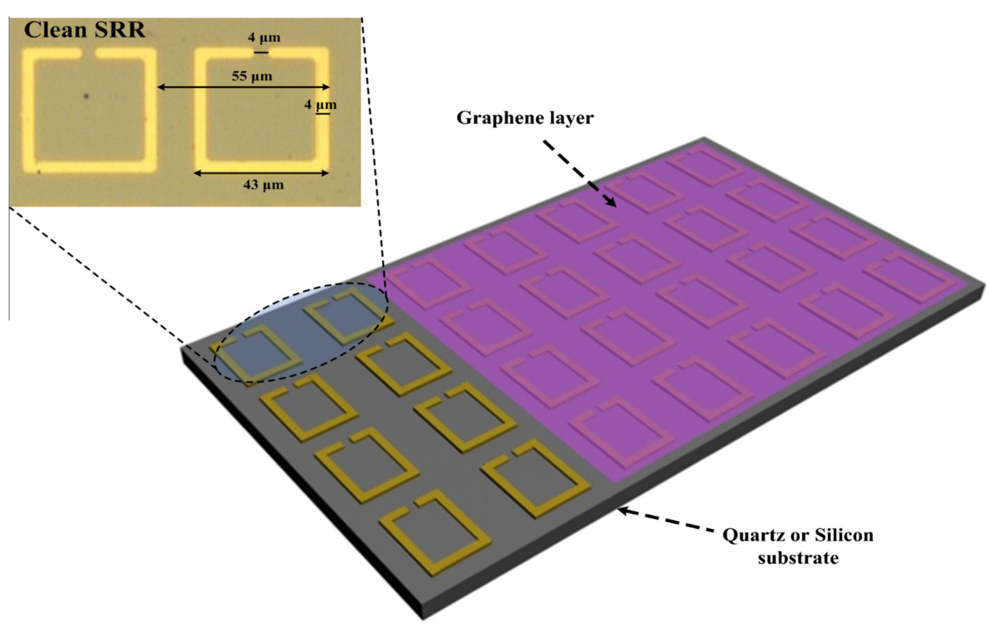

Fig. 1 – Schematic of graphene–SRRs hybrid structure. Top-left shows the optical image of SRRs and structural parameters of SRRs. (A color version of this figure can be viewed online.)

decreased 2D mode. This is due to the reason that N as foreign atoms can largely change the lattice of the pristine graphene and tune its molecular bond properties [25]. The low conductivity of N-doped graphene has already been proven in our previous work, leading to a low intraband carrier concentration. The inset is the optical image at the collection-point for Raman spectrum. Owing to the enhancement by SRRs [18], Raman scattering of graphene increased with good signal-to-noise ratio (SNR). The difference between the Raman spectra of graphene samples on SRRs and Si substrates is shown in Fig. S3 in Supplementary Material. Raman multiple spot analysis is employed to reveal the uniformity and continuity of our graphene overlayers (shown in Fig. S4, S5 and S6 in Supplementary Material).

THz responses of SRRs on Si and SiO_2 substrate before and after graphene deposition were measured by a custom-designed THz-TDS system as shown in Fig. S7 in Supplementary Material (Ti:Sapphire femtosecond laser: MaiTai Spectra-Physics, repetition rate 80 MHz, pulse width 70 fs, central wavelength 800 nm).

3. Results and discussion

3.1. *THz response and simulation*

In our previous work [25], flat and characterless THz responses of pristine graphene and N-doped graphene have been obtained. The pristine graphene shows the THz transmission of ~0.73 in our effective frequency region, while the N-doped graphene with 3.1 (NG1) and 4.7 (NG2) atomic percent doping concentration show 0.95 and 0.97 in THz region, respectively. Graphene–SRRs and N-doped graphene–SRRs hybrids exhibit remarkable spectral response variations. When the polarization of the incident THz wave was parallel to the gap-bearing side of SRRs, the THz transmission responses of SRRs before and after graphene deposition on different substrates were shown in Fig. 3(a) and (c). In Fig. 3(a), the THz transmission responses of graphene–SRRs and N-doped graphene–SRRs hybrid structures on Si substrate reveal two resonant responses in SRRs, corresponding to low frequency resonant mode (LFRM) at ~0.4 THz and high frequency resonant mode (HFRM) at ~1.2 THz. LFRM is related to the circular transient current induced by the incident THz field and can be explained by an inductance-capacitance (LC) oscillator model (31), while HFRM is a plasmonic resonance described by a plasmonic dipole resonance [32].

For graphene–SRRs hybrid structure, THz transmission at LFRM is increased from 8.8% to 18.6% ($\Delta T = 9.8\%$), with a strong red-shift in resonant region from 0.413 to 0.346 THz ($\Delta f = 0.067$ THz). The THz transmission at HFRM is increased from 1.8% to 12.9% ($\Delta T = 11.1\%$) and its resonant frequency shifts from 1.225 to 1.096 THz ($\Delta f = 0.129$ THz). Meanwhile, a remarkable broadening for LFRM and HFRM can be observed. On the other hand, the N-doped graphene–SRRs hybrid

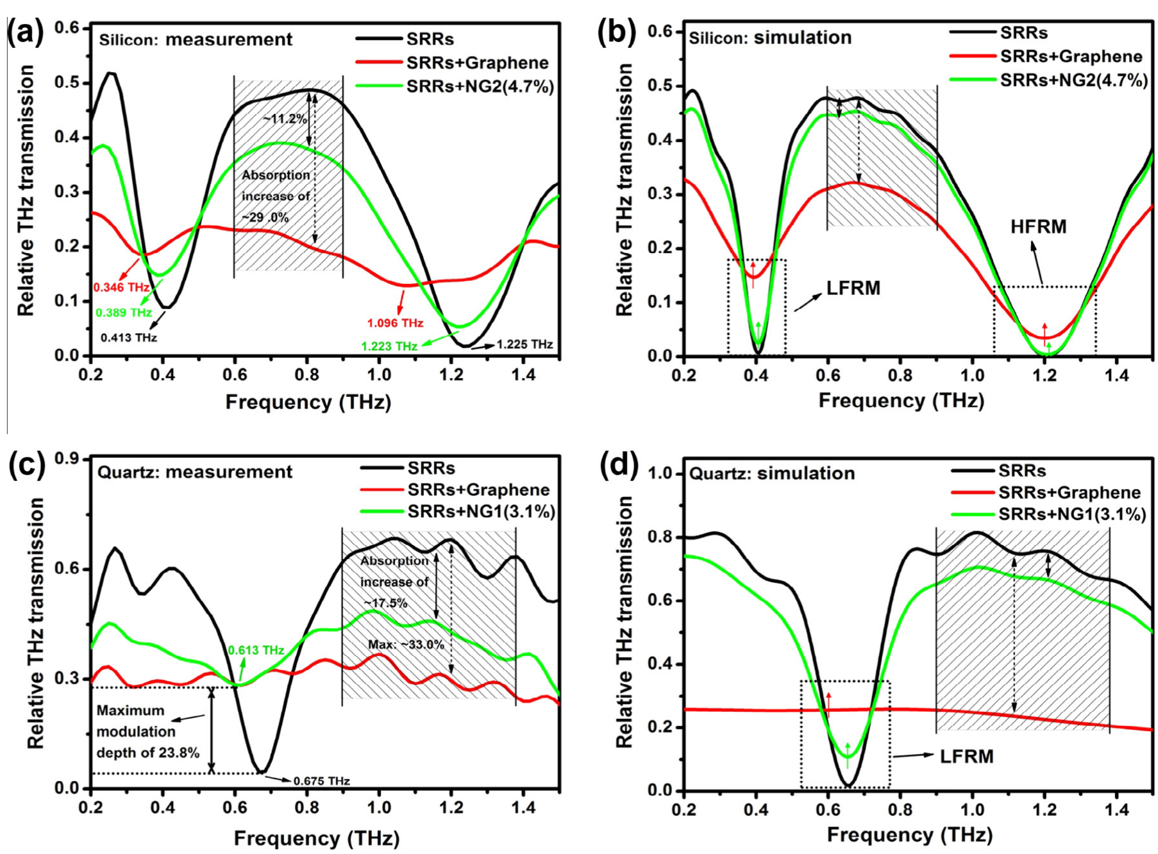

Fig. 3 – THz transmission of graphene–SRRs and N-doped graphene–SRRs hybrid structures on Si substrate (a) and SiO_2 substrate (c). Simulated THz transmission of the presented hybrid structures on Si substrate (b) and SiO_2 substrate (d). The black shadow shows the non-resonant region of graphene–SRRs and N-doped graphene–SRRs hybrid structures. (A color version of this figure can be viewed online.)

structure has a relatively weak variation in resonant region. THz transmission at LFRM is increased from 8.8% to 14.8% ($\Delta T = 5.0\%$) and its resonant frequency shifts from 0.389 to 0.413 THz ($\Delta f = 0.024$ THz). The THz transmission at HFRM increases from 1.8% to 5.4% ($\Delta T = 3.6\%$) with a broadening and a red-shift (from 1.225 to 1.223 THz, $\Delta f = 0.002$ THz). Fig. 3(c) shows the THz transmission response of graphene–SRRs and N-doped graphene–SRRs hybrid structures on SiO_2 substrate. N-doped graphene–SRRs shows the similar variation tendency as shown in Fig. 3(a). There is an increase of transmission at LFRM from 4.5% to 28.3% ($\Delta T = 23.8\%$), a red-shift in resonant region from 0.675 to 0.613 THz ($\Delta f = 0.062$ THz) and a broadening in resonant region at LFRM. However, after pristine graphene deposition onto the SRRs/SiO2 surface, THz resonance response at LFRM is smoothed due to the efficient coupling between graphene on metamaterials and SiO_2 surfaces. Owing to the bandwidth limitation of our THz-TDS system, the SNR becomes worse after 1.5 THz and the HFRM at ~2 THz is out of the range of our experiments.

On the basis of these observations, the graphene overlayer clearly shows the ability to largely modulate the THz absorption response of SRRs in the non-resonant response region. As shown in the black shadow in Fig. 3(a) and (c), the non-resonant spectral response region of both graphene–SRRs and N-doped graphene–SRRs hybrid structures show flat and broadband enhancements in THz absorption response. For Si substrate, the average THz transmission response of graphene–SRRs in the non-resonant region (from 0.6 to 0.9 THz) decreases from 49.1% to 20.1% (enhancement of 29.0%). N-doped graphene–SRRs has a relatively weak THz absorption response enhancement of 11.2%. For SiO_2 substrate, graphene–SRRs shows the maximum THz absorption enhancement of 33.0% (THz transmission response decreases from 64.5% to 31.5%) in the non-resonant response region (from 0.9 to 1.38 THz). N-doped graphene–SRRs on SiO_2 substrate shows the THz absorption response enhancement of 17.5%. It is worth noting that the significant difference of THz response enhancements in non-resonant region of SRRs has strong correlation with the conductivity of overlayer, namely the varied conductivity of graphene overlay is responsible for the changes in THz response. The results indicate the promising prospects of the graphene–SRRs hybrid structure used as the broadband THz photodetector or other THz functional devices for THz wave manipulation.

In addition, the THz transmission of SRRs before and after the graphene deposition were also measured with the polarization of the incident THz wave perpendicular to the gap-bearing side of SRRs (Fig. S9 in Supplementary Material). With the overlayer, the same spectral variation tendency can be noticed no matter the polarization of the incident THz wave is parallel or perpendicular to the gap-bearing side of SRRs. However, when the polarization of the incident THz wave is perpendicular to the gap-bearing side of SRRs, the presented hybrid structure shows slight spectral change including the red-shift of the resonant frequency, the broadening of the resonant peak and the THz transmission response variation in the resonant region. This could be attributed to the novel resonance electric field distribution of SRRs induced by certain polarization of the incident THz wave.

Numerical simulations with the same structure have been conducted with periodic boundary conditions (CST Microwave Studio) [33]. The overlayer has been modeled by a dielectric layer with the thickness $t = 1$ nm in Zou's work [22]. We have subsequently decreased t until we found that the limit $t \to 0$ is fully converged in our simulations at the thickness of $t = 1$ nm. The used electrical conductivity of graphene and N-doped graphene overlayers on both Si and SiO_2 substrate obtained by four point probe measurements (Beijing ZXYD Technology Ltd TZH24-RTS-9) are $\sigma_{\text{grap-Si}} = 4.47 \times 10^5$ S/m, $\sigma_{\text{NG2-Si}} = 5.29 \times 10^4$ S/m, $\sigma_{\text{grap-SiO}_2} = 1.5 \times 10^6$ S/m, and $\sigma_{\text{NG1-SiO}_2} = 8.04 \times 10^4$ S/m, respectively. The simulated THz transmission response of hybrid structures on both Si and SiO_2 substrate are shown in Fig. 3(b) and (d). These numerical simulations can capture the main characteristics of the experiments such as the red-shift of the resonant frequency, the broadening of the resonant mode, and the THz transmission response variation in the resonant and non-resonant THz response region.

The corresponding electric field distribution of SRRs at LFRM without overlayer on Si and SiO_2 substrates are shown in Fig. 4(a) and (b). LFRM can be explained by an inductance-capacitance (LC) oscillator model. The resonant frequency can be defined as: $f_{\text{LFRM}} = 1/2\pi\sqrt{\text{LC}}$. Where the inductance L is determined mainly by the geometry of SRRs and the capacitance C is highly relevant to both the gap dimension and the surrounding medium [31]. With the introduction of graphene or N-doped graphene, the total permittivity increases and results in the increase of SRRs total capacitance, which cause the red-shift of LFRM. Significantly, the degree of the red-shift depends on the dielectric property of the overlayer near the gap of SRRs. In THz region, graphene materials have proved to follow Drude model [34] as: $\varepsilon \approx -\sigma_{\text{DC}}/(\varepsilon_0\Gamma) + i\sigma_{\text{DC}}/(\varepsilon_0\omega)$ [35]. Where σ_{DC} is the electrical conductivity of graphene materials, Γ is damping rate and ε_0 is the vacuum permittivity. The value of the permittivity of graphene in THz region is quite larger than that in visible-infrared region and that of N-doped graphene. It causes quite larger red-shift of the LFRM of SRRs with graphene than with N-doped graphene.

HFRM is a diluted plasmonic resonance, which can be approximately described by a plasmonic dipole with the resonant frequency at $f_{\text{HFRM}} \approx 1/(4\pi d\sqrt{\varepsilon_{\text{ave}}})$ [31]. Where d is the length of SRRs arm and ε_{ave} is the average permittivity of the surrounding medium. The simulated electric field distribution of SRRs at HFRM without overlayer on Si and SiO_2 are shown in Fig. 4(c) and (d). When graphene or N-doped graphene deposit on the surface of SRRs, the ε_{ave} would increase, resulting in the red-shift of the HFRM [36]. Similar to LFRM, due to the quite large permittivity of graphene materials in THz region, the average permittivity of the surrounding medium of SRR (ε_{ave}) is largely increased by the graphene overlayer and causes the obvious red-shift of HFRM. With the deposition of the overlayer, a strong depolarization field is formed around SRRs, which restricts the movement of electrons in the SRRs driven by the incident THz field [37,38]. Unlike the LFRM, the HFRM is highly relevant to the surrounding micro-environment dielectric variation, giving rise to larger red-shift of the HFRM.

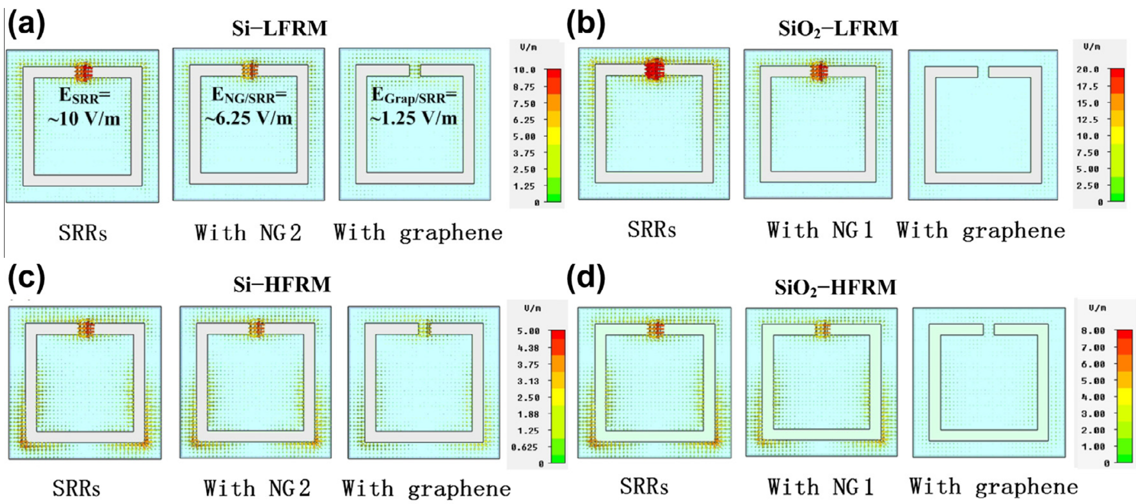

Fig. 4 – Simulated electric field distribution at LFRM of SRRs without overlayer and with different graphene overlayers on Si (a) and SiO_2 (b) substrate. Simulated electric field distribution at HFRM of SRRs without overlayer and with different graphene overlayers on Si (c) and SiO_2 (d) substrate. (A color version of this figure can be viewed online.)

Optical conductivity in graphene involves two processes: carrier intraband transitions and interband transitions. In THz region, optical conductivity is mainly affected by the carrier intraband transitions in graphene [15]. After the overlayer deposits onto SRRs, the graphene or N-doped graphene could make the positive and negative charges near the gap of SRRs neutralize, leading to the decrease of the electric field intensity near the gap of SRRs at resonant mode. Fig. 4(a) shows the electric field distribution at LFRM of SRRs without overlayer and with different graphene overlayers on Si substrate. With the overlayers deposition, the resonance electric field intensity of SRRs at LFRM is largely reduced. For the N-doped graphene as overlayer, the resonance electric field intensity of SRRs at LFRM is modulated from 10 to 6.25 V/m ($\Delta E_{NG} = -3.75$ V/m). For the pristine graphene as overlayer, the resonance electric field intensity is modulated from 10 to 1.25 V/m ($\Delta E_{Grap} = -8.75$ V/m). Compared with N-doped graphene overlayer, the pristine graphene shows double modulation depth in the electric field intensity of SRRs ($\Delta E_{Grap}/\Delta E_{NG} = \sim 2.3$). This is consistent with the modulation depth in the THz transmission response at LFRM ($\Delta T_{Grap\text{-}LFRM}/\Delta T_{NG\text{-}LFRM} = 9.7\%/5.0\% = 1.94$) as shown in Fig. 3(a). This would explain the increase of THz transmission response of graphene–SRRs and N-doped graphene–SRRs hybrid structure at resonant mode. Significantly, the increase of THz transmission at resonant mode is direct proportion to the electrical conductivity of overlayer due to the neutralization of positive and negative charges near the gap of SRRs.

However, to a certain extent, there is some deviation between the simulation and the experiments, such as the red-shift degree of the resonant frequency, the broadening degree of the resonant mode and the modulation depth of the THz transmission response in the resonant and non-resonant response region. The deviation of the numerical simulations could be from the reason that the calculations ignore the charge-transfer between the graphene and metamaterials. As soon as graphene contacts with metamaterials fabricated with Au, electrons are transferred from graphene to Au and graphene is *p*-type doped on Au [39]. This effect is important and can further shift the Fermi level of graphene, causing the variation of the graphene electrical conductivity [39].

3.2. *Coupling mechanism of metamaterials and graphene*

As shown in Fig. 5(a), a coupling model has been proposed to quantitatively reveal the interaction mechanism between graphene and SRRs in THz region. Similar to carbon nanotubes as overlayer [40], the mechanical oscillator is driven by an external harmonic force *F* (THz field). The behavior of this coupling model can be described by the following equation:

$$M_1\frac{d^2x_1}{dt^2} = F - K_1x_1 - K_c(x_1 - x_2) - \Gamma\frac{dx_1}{dt} \quad (1)$$

$$M_2\frac{d^2x_2}{dt^2} = F - K_2x_2 + K_c(x_1 - x_2) - \Gamma_{add}\frac{dx_2}{dt} \quad (2)$$

More details about Eqs. (1) and (2) are shown in the Supplementary Material. Here, the resonance of SRRs is represented by the oscillation with a mass M_1 and the spring constant K_1, while a mass M_2 and spring constant K_2 for graphene overlayer. M_1 represents excitations in the gap of SRRs and M_2 represents carrier excitations in graphene overlayer. The coupling of graphene overlayer and SRRs is represented by the spring constant K_c. Friction Γ represents the damping of SRRs and this damping mainly affects the resonant bandwidth in the spectral response [41]. With the coupling of graphene and SRRs, an additional damping (Γ_{add}) is introduced, which leads to the broadening as shown in Fig. 5(b) and (c). Γ_{add} is highly relevant to the permittivity of overlayers [42]. Fig. 5(b) and (c) are obtained by solving Eqs. (1) and (2) under the initial values of $M_1 = 1$, $M_2 = 4.4$, $K_1 = 1$, $K_2 = 3.9$, $K_c = 1.1$, $\Gamma = 0.001$, $\Gamma_{add} = 0.45$. According to the analyses shown in Fig. 5(b) and (c), the variation of THz intensity in resonant region is consistent with the experimental observation of increased THz

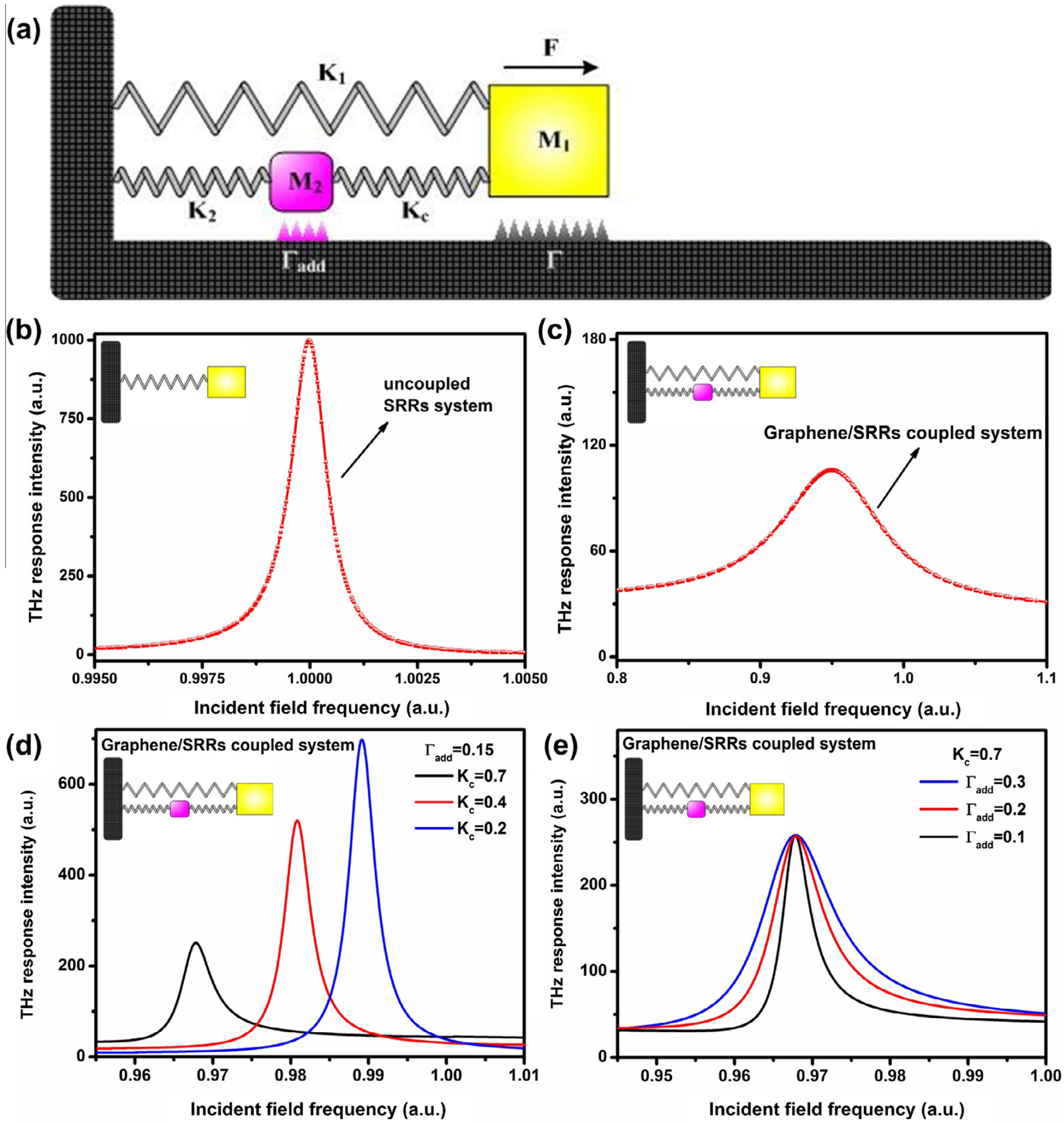

Fig. 5 – (a) Illustrative coupling model of the interaction between graphene and SRRs. This oscillator model is driven by an external harmonic force F (THz field). The resonance of SRRs is represented by the oscillation with a mass M_1, while the graphene overlayer is represented by a mass M_2. K_1 and K_2 are the spring constants of the oscillator M_1 and M_2, respectively. K_c represents the coupling of graphene overlayer with SRRs. The friction Γ represent the damping of SRRs, while Γ_{add} is an additional damping introduced by the graphene overlayers. (b) and (c) THz response intensity of the uncoupled SRRs and the graphene–SRRs coupled system. (d) THz spectra of graphene–SRRs coupled system under the different coupling strength K_c while keeping the damping constant Γ_{add} = 0.15 and other parameters constant. (e) THz spectra of graphene–SRRs coupled system under different damping constant Γ_{add}, while keeping the coupling strength K_c = 0.7 and other parameters constant. (A color version of this figure can be viewed online.)

transmission of graphene–SRRs hybrid structure in Fig. 3(a). The THz response in off-resonant region shows increased THz absorption. A red-shift can also be observed in THz intensity spectra (Fig. 5(c)), corresponding to the experimental results in Fig. 3(a) and (c).

To understand the influence from the coupling and damping of graphene with metamaterials, we further modulate the parameters K_c and Γ_{add} as shown in Fig. 5(d) and (e), while keeping other parameters constant. It is evident that K_c determines both frequency shift and the intensity of the resonance, that is, the stronger coupling leads to the larger red-shift and lower peak intensity. Γ_{add} mainly determines the shape of the resonance as well as the bandwidth of the resonance with the higher damping for broader spectral response.

Further calculations suggest that the THz peak intensity is exponential decay with the K_c (black dots and curve in

Fig. 6(a)). However, the THz intensity in off-resonant region is exponential growth with the K_c (blue dots and curve in Fig. 6(a)). The red curve shows the linear proportion dependency between the red-shift frequency and K_c. Fig. 6(b) shows an exponential increasing of bandwidth with Γ_{add}. This is consistent with our experimental measurements and other measurements for the similar carrier coupling between graphene and metamaterials [19]. The results from Fig. 6 also show the similar spectral response and the magnitude variation tendency for the interband carrier coupling [20–22].

Valmorra et al. [19] proposed a voltage-tunable coupling of graphene with metamaterials and analyzed the data with the lumped-element circuit modes, in which clear intensity variation but less frequency shift were observed. This implied that the voltage-tunability may be determined by K_c, not Γ_{add}, which is consistent with our results shown in Fig. 6. However, with the graphene in infrared photonic metamaterials, Papasimakis et al. [20] found a strong red-shift of the resonance as well as broadening, suggesting the contributions of both K_c and Γ_{add}. The coupling model presented here could help further understanding of the carrier coupling between graphene and metamaterials.

Fig. 7 shows simulated THz transmission response of SRRs covered by graphene overlayers with different electrical conductivity on both Si (a) and SiO_2 (b) substrate. The minimum electrical conductivity in our simulation is set to the minimum electrical conductivity in our experiments, corresponding to $\sigma_o = \sigma_{NG3\text{-}Si} = 5.29 \times 10^4$ S/m. The electrical conductivity of the overlayer is changed from $3\sigma_o$ to $26\sigma_o$ as shown in Fig. 7. We focus on both resonant and non-resonant THz response region and define the parameters I_{LFRM}, I_{HFRM}, and I_{non} to reveal the variation of THz response with the change of the electrical conductivity. I_{LFRM} is employed to describe the variation of LFRM at resonance and $I_{LFRM} = T_{LFRM} - T_{set}$, where T_{LFRM} represents the THz transmission of overlayer–SRRs at LFRM. T_{set} is the THz transmission of overlayer–SRRs hybrid structure at the fixed frequency (0.6 THz for Si substrate and 1.0 THz for SiO_2 substrate). I_{non} is employed to describe the THz absorption variation in the non-resonant response region, corresponding to $I_{non} = T_{SRRs} - T_{ave}$. Where T_{SRRs} is the average of THz transmission of SRRs without overlayer in the non-resonant response region and T_{ave} is the average of THz transmission of overlayer–SRRs hybrid structure in the non-resonant response region. The non-resonant response region ranges from 0.6 to 0.9 THz for Si substrate and from 0.9 to 1.38 THz for SiO_2 substrate as shown in the black shadow area of Fig. 7(a) and (b). The highly sensitive response of the $\sigma_{overlayer}$ with I_{LFRM} can be expressed by an exponential fitting for both SRRs on Si and SiO_2 substrate (Fig. 7(c)). The response on SiO_2 is more sensitive than that on Si due to the substrate effect with metamaterials [43].There are two interfaces between graphene and metamaterials in a microscopic level. One is the interface between graphene and the substrate (In our experiment metamaterials are thoroughly covered by graphene and the extra parts of graphene overlayer will contact with substrate) and the other is the interface between the graphene and the Au pattern. When a graphene sheet directly contacts with a dielectric substrate, the electrons in graphene along the interface will couple to the electric field induced by the surface phonon mode of the dielectric substrate. This causes a remote electron–phonon interaction generated at the interface between graphene and substrate [44,45]. This interaction can be described by a Hamiltonian [46]: $H_{e-ph} = \sum_{\vec{q}} M_{\vec{q}} \rho_{\vec{q}} (b^{\dagger}_{\vec{q}} + b_{-\vec{q}})$, where $b^{\dagger}_{\vec{q}}$ and $b_{-\vec{q}}$ represent the creation and annihilation operators for the surface phonons of substrate with momentum $\vec{q}$ parallel to the graphene-substrate interface. $\rho_{\vec{q}}$ is the graphene electron density operator. The previous work has already proven that this remote scattering with the substrate phonons is the main limiting factor of the carrier mobility in graphene through the solution of the Hamiltonian. This corresponds to the polarizability of the substrate material [46]. The polarizability of material (χ_e) is relevant to its permittivity (ε) and the relationship can be described by $\varepsilon = (1 + \chi_e)\varepsilon_0$. In our experiment, the permittivity of Si substrate (11.4) is much larger than SiO_2 substrate (3.84). Thus, it would explain the

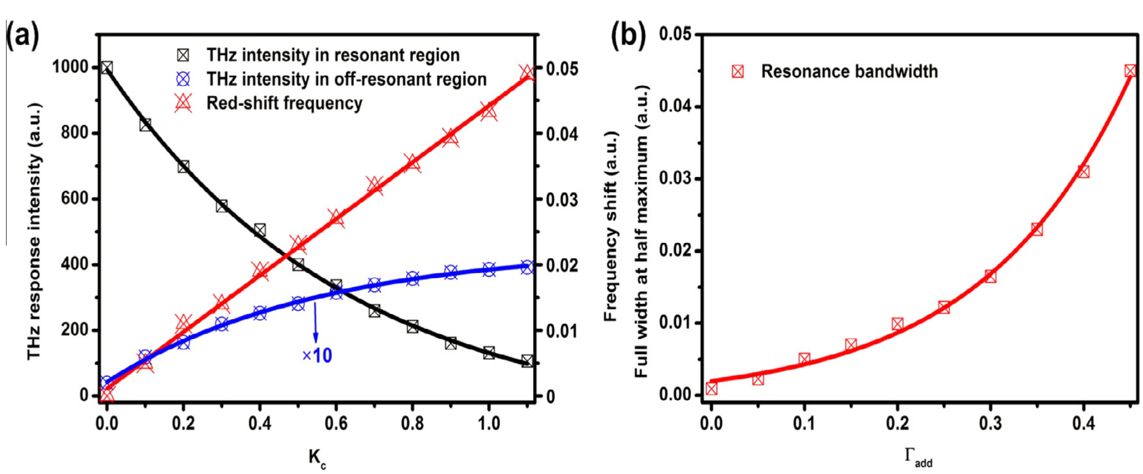

Fig. 6 – (a) Dependency between THz intensity in resonant region and K_c (black dots). Dependency between THz intensity in off-resonant region and K_c (blue dots). The curves are the exponential fitting. Dependency between the red-shift frequency and K_c (red dots). The curves are the linear fitting. (b) Dependency between bandwidth and Γ_{add}. The curves are the exponential fitting. (A color version of this figure can be viewed online.)

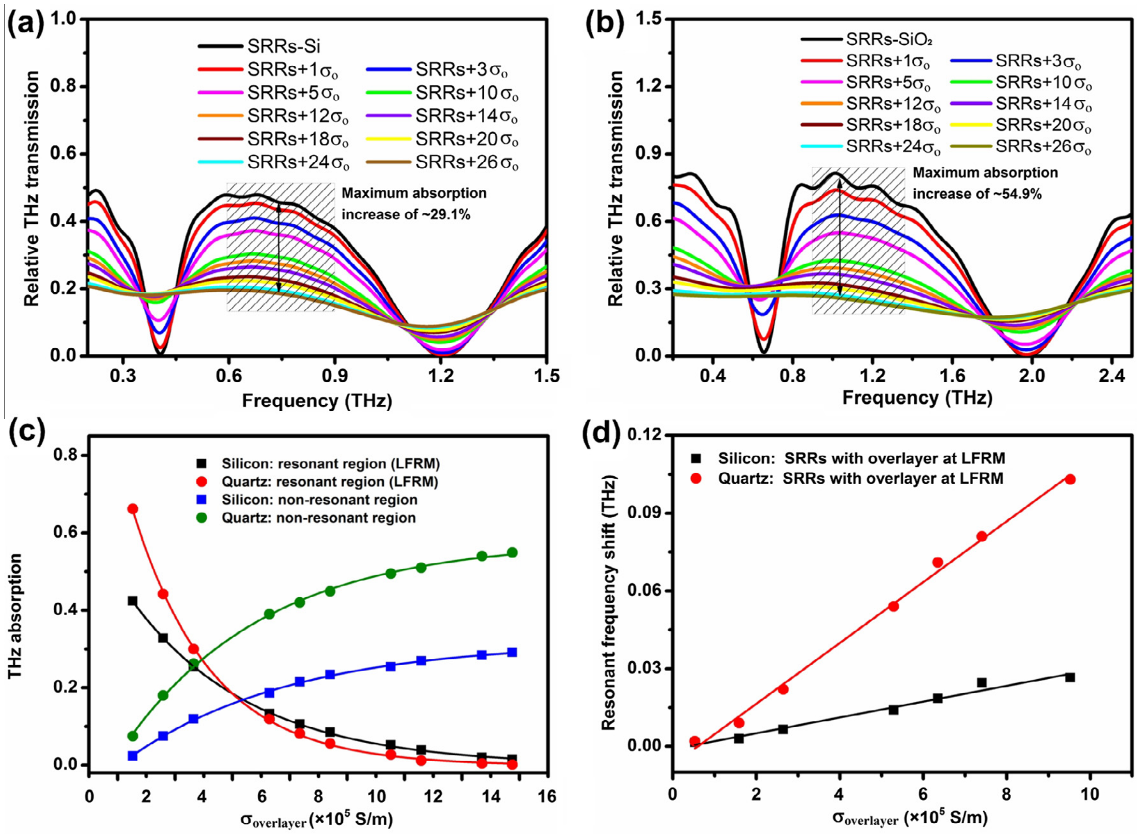

Fig. 7 – Simulated THz transmission response of SRRs covered by graphene overlayers with different electrical conductivity on Si (a) and SiO_2 (b) substrate in both resonant and non-resonant response region. The electrical conductivity for overlayers is set to the multiple of σ_o. Here, σ_o is the minimum electrical conductivity in the experiment, corresponding to $\sigma_o = \sigma_{NG3\text{-}Si} = 5.29 \times 10^4$ S/m. Black shadow area shows the maximum THz absorption increase of graphene–SRRs hybrid structure in the non-resonant region. (c) Simulated THz transmission response of graphene–SRRs hybrid structure with the electrical conductivity of overlayers. The solid lines are the exponential fitting. (d) Dependency between the resonant frequency shift (Δf) of LFRM and the overlayer electrical conductivity. The solid lines are the linear fitting. (A color version of this figure can be viewed online.)

quite larger carrier mobility of graphene overlayer contacted with SiO_2 substrate than that with Si substrate. On the other hand, when the graphene sheet directly contact with SiO_2 substrate, the surface oxygen dangling bonds of SiO_2 substrate could bind to graphene through the formation of the C–O bonds, causing the charge transfer from graphene to the oxygen dangling bonds [47]. This charge-transfer interaction between graphene and SiO_2 substrate could induce *p*-type doping, resulting in the increase of the carrier concentration in graphene. The modulation of the carrier mobility and carrier concentration in graphene will further modulate the electrical conductivity of graphene overlayer. This also can be supported by the electric field pattern difference at LFRM of graphene–SRRs hybrid structure on Si and SiO_2 substrate as shown in Fig. 4(a) and (b). Based on these, we suggest the remote phonon scattering and charge-transfer effect could influence the properties of the carrier dynamics in graphene, which cause the variation of the electrical conductivity of graphene overlayer. This will result in the influences of the intraband carrier coupling between graphene and SRRs in THz region. Since the electrical conductivity of graphene can be tuned by absorbed molecules such as NO_2 [48], NH_3 [49], HNO_3 [50], F_4-TCNQ [51], the results in Fig. 7(c) also suggested that this kind of hybrid structure can be used as high sensitive conductivity sensor.

The relationship between the I_{non} and $\sigma_{overlayer}$ is also shown in Fig. 7(c). The highly dependency between I_{non} and $\sigma_{overlayer}$ can be well fitted by an exponential growth function. Especially for the graphene–SRRs hybrid structure on SiO_2 substrate, it shows the remarkable THz absorption enhancement in non-resonant region. The corresponding absorption increase of ~54.9% is shown in Fig. 7(b). Even though our experimental data exhibit broadband THz absorption enhancement of ~33.0% (Fig. 3(c)), this could be optimized under ideal circumstance for maximum electrical conductivity of graphene. So far the maximum electrical conductivity measurements of graphene can reach 2.35×10^7 S/m [52]. Compared with the response of pristine graphene [9,15], this graphene–SRRs hybrid structure shows more than twice as much THz absorption as the pristine one. This excellent THz enhancement means the coupling between graphene and SRRs can largely increase THz response of both graphene and SRRs, which achieve win–win characteristics. This will also increase THz wave detection responsivity with the graphene–SRRs hybrid structure and exhibits an excellent application prospect in THz photodetection. Similar results for HFRM mode are shown in Supplementary Material Fig. S10.

Meanwhile, the dependency between the resonant frequency shift (Δf) of LFRM and the overlayer electrical conductivity ($\sigma_{\mathrm{overlayer}}$) are shown in Fig. 7(d). The data in Fig. 7(d) demonstrate a linear relationship. The higher degree of Δf and $\sigma_{overlayer}$ for SiO_2 compared with Si suggests that the lower the dielectric constant of substrate is, the better the sensitivity will be. This also proves that the coupling between graphene and SRRs is also influenced by the substrate caused by the difference of the substrate permittivity. More explanations for the frequency shift and the permittivity difference can be found in Eq. (3) in Supplementary Material.

Comparing Figs. 6(a) and 7(c), the THz intensity in resonant region shows the similar exponential decay with the K_c as well as the $\sigma_{\mathrm{overlayer}}$. The THz intensity in off-resonant region shows the similar exponential increase with K_c (Fig. 6(a)) compared to $\sigma_{\mathrm{overlayer}}$ (Fig. 7(c)). The red-shift frequency of the THz intensity spectra also shows the similar linear increase with K_c (Fig. 6(a)) compared to $\sigma_{\mathrm{overlayer}}$ (Fig. 7(d)). This suggests that the coupling parameter K_c is highly related to the conductivity of graphene $\sigma_{\mathrm{overlayer}}$ and the variation of K_c is equivalent to the modulation of graphene overlayer electrical conductivity. The coupling model also agrees well with both experimental measurements (Fig. 3(a) and (c)) and numerical simulations (Fig. 7) for further understanding the hybridization of metamaterials and graphene.

4. Conclusion

In this paper, we demonstrate a graphene–SRRs hybrid structure based on a large-area graphene and N-doped graphene synthesized by APCVD. Hybridization of graphene and N-doped graphene with SRRs leads to an intraband carrier coupling between graphene and SRRs in THz region. A coupling model and the numerical calculation are employed to reveal this coupling in THz region. The results suggest the coupling is highly relevant to the electrical conductivity of graphene overlayer. THz response in resonant region shows exponential decay with the electrical conductivity of graphene overlayer, while the THz response in non-resonant region shows exponential growth with the electrical conductivity of graphene overlayer. Moreover, the resonant frequency shift shows exponential increasing with the electrical conductivity of graphene overlayer. Correspondingly, the change of this coupling under the modulation of this electrical conductivity always realize through the coupling strength K_c and damping constant Γ_{add} in our coupling oscillator model. In our model, K_c determines both frequency shift as well as the intensity of the resonance. Γ_{add} mainly determines the shape of the resonance as well as the bandwidth of the resonance. Also, substrates could bring the remote phonon scattering, charge transfer, and dielectric effect, which show the influence such as low dielectric constant for high coupling. The coupling model as well as the numerical simulations could provide some clues to optimize the interaction between graphene and metamaterials. This work could pave the way for the potential applications of graphene–metamaterial hybridation for high efficient THz devices.

Acknowledgments

This work was supported by National Natural Science Foundation of China (Nos. 61275105, 11374240, 61177059, 61390503, 51272278, 51103175), Ph.D. Programs Foundation of Ministry of Education of China (No. 20136101110007), Natural Science Basic Research Plan in Shaanxi Province of China (No. 2012KJXX-27), Key Laboratory Science Research Plan of Shaanxi Education Department (13JS101), National Basic Research Program of China (Nos. 2014CB339800, 201410780), the Knowledge Innovation Project of CAS (No. KJCX2-EW-W02).

Appendix A. Supplementary data

Supplementary data associated with this article can be found, in the online version, at http://dx.doi.org/10.1016/j.carbon.2014.06.053.

REFERENCES

[1] Ferguson B, Zhang XC. Materials for terahertz science and technology. Nat Mater 2002;1:26–33.

[2] Bolotin KI, Sikes KJ, Jiang Z, Klima M, Fudenberg G, Hone J, et al. Ultrahigh electron mobility in suspended graphene. Solid State Commun 2008;146:351–5.

[3] Novoselov K, Fal V, Colombo L, Gellert P, Schwab M, Kim K. A roadmap for graphene. Nature 2012;490:192–200.

[4] Bonaccorso F, Sun Z, Hasan T, Ferrari A. Graphene photonics and optoelectronics. Nat Photon 2010;4:611–22.

[5] Nair R, Blake P, Grigorenko A, Novoselov K, Booth T, Stauber T, et al. Fine structure constant defines visual transparency of graphene. Science 2008;320:1308.

[6] Lim GK, Chen ZL, Clark J, Goh RG, Ng WH, Tan HW, et al. Giant broadband nonlinear optical absorption response in dispersed graphene single sheets. Nat photon 2011;5:554–60.

[7] Choi H, Borondics F, Siegel DA, Zhou SY, Martin MC, Lanzara A, et al. Broadband electromagnetic response and ultrafast dynamics of few-layer epitaxial graphene. Appl Phys Lett 2009;94:172102.

[8] Dawlaty JM, Shivaraman S, Strait J, George P, Chandrashekhar M, Rana F, et al. Measurement of the optical absorption spectra of epitaxial graphene from terahertz to visible. Appl Phys Lett 2008;93:131905.

[9] Zhou Y, Xu X, Fan H, Ren Z, Bai J, Wang L. Tunable magnetoplasmons for efficient terahertz modulator and isolator by gated monolayer graphene. Phys Chem Chem Phys 2013;15:5084–90.

[10] Winnerl S, Orlita M, Plochocka P, Kossacki P, Potemski M, Winzer T, et al. Carrier relaxation in epitaxial graphene photoexcited near the Dirac point. Phys Rev Lett 2011;107:237401.

[11] Grigorenko A, Polini M, Novoselov K. Graphene plasmonics. Nat Photon 2012;6:749–58.

[12] Vicarelli L, Vitiello M, Coquillat D, Lombardo A, Ferrari A, Knap W, et al. Graphene field-effect transistors as room-temperature terahertz detectors. Nat Mater 2012;11:865–71.

[13] Muraviev AV, Rumyantsev SL, Liu G, Balandin AA, Knap W, Shur MS. Plasmonic and bolometric terahertz detection by

graphene field-effect transistor. Appl Phys Lett 2013;103:181114.

[14] Zhou Y, Xu X, Fan H, Ren Z, Chen X, Bai J. Tunable magneto-optical kerr effect in gated monolayer graphene in terahertz region. J Phys Soc Jpn 2013;82:4717.

[15] Sensale-Rodriguez B, Yan R, Kelly MM, Fang T, Tahy K, Hwang WS, et al. Broadband graphene terahertz modulators enabled by intraband transitions. Nat commun 2012;3:780.

[16] Kurita Y, Kobayashi K, Otsuji T, Ducournau G, Meziani Y.M, Popov V.V, et al. In: Extremely-high sensitive terahertz detector based on dual-grating gate InP-HEMTs, Indium phosphide and related materials (IPRM), 2013 International Conference on, 19–23 May 2013.

[17] Shalaev VM. Optical negative-index metamaterials. Nat photon 2007;1:41–8.

[18] Sarau G, Lahiri B, Banzer P, Gupta P, Bhattacharya A, Vollmer F, et al. Enhanced Raman scattering of graphene using arrays of split ring resonators. Adv Opt Mater 2013;1:151–7.

[19] Valmorra F, Scalari G, Maissen C, Fu W, Schonenberger C, Choi JW, et al. Low-bias active control of terahertz waves by coupling large-area CVD graphene to a terahertz metamaterial. Nano Lett 2013;13:3193–8.

[20] Papasimakis N, Luo Z, Shen ZX, De Angelis F, Di Fabrizio E, Nikolaenko AE, et al. Graphene in a photonic metamaterial. Opt Express 2010;18:8353–9.

[21] Nikolaenko AE, Papasimakis N, Atmatzakis E, Luo Z, Shen ZX, De Angelis F. Nonlinear graphene metamaterial. Appl Phys Lett 2012;100:181109.

[22] Zou Yanhong, Tassin Philippe, Koschny Thomas, Soukoulis1 Costas M. Interaction between graphene and metamaterials: split rings vs. wire pairs. Opt Express 2012;20:12198–204.

[23] Lee SH, Choi M, Kim TT, Lee S, Liu M, Yin X, et al. Switching terahertz waves with gate-controlled active graphene metamaterials. Nat Mater 2012;11:936–41.

[24] Wu J, Shi W, Chopra N. Optical properties of gold/multilayer-graphene/carbon nanotube hybrid materials. Carbon 2014;68:708–17.

[25] Li JY, Ren Z, Zhou Y, Wu X, Xu X, Qi M, et al. Scalable synthesis of pyrrolic N-doped graphene by atmospheric pressure chemical vapor deposition and its terahertz response. Carbon 2013;62:330–6.

[26] Lherbier A, Blase X, Niquet YM, Triozon F, Roche S. Charge transport in chemically doped 2D graphene. Phys Rev Lett 2008;101:036808.

[27] Deifallah M, McMillan PF, Cora F. Electronic and structural properties of two-dimensional carbon nitride graphenes. J Phys Chem C 2008;112:5447–53.

[28] Wei D, Liu Y, Wang Y, Zhang H, Huang L, Yu G. Synthesis of N-doped graphene by chemical vapor deposition and its electrical properties. Nano Lett 2009;9:1752–8.

[29] Wagner C, Muilenberg G. Handbook of X-ray photoelectron spectroscopy. Perkin-Elmer; 1979.

[30] Ferrari AC, Meyer JC, Scardaci V, Casiraghi C, Lazzeri M, Mauri F, et al. Raman spectrum of graphene and graphene layers. Phys Rev Lett 2006;97:187401.

[31] Padilla WJ, Taylor AJ, Averitt RD. Dynamical electric and magnetic metamaterial response at terahertz frequencies. Phys Rev Lett 2006;96:107401.

[32] Pendry J, Holden A, Robbins D, Stewart W. Magnetism from conductors and enhanced nonlinear phenomena. IEEE T Microw Theory 1999;47:2075–84.

[33] Lu X, Zhang W. Terahertz localized plasmonic properties of subwavelength ring and coaxial geometries. Appl Phys Lett 2009;94:181106.

[34] Horng J, Chen CF, Geng B, Girit C, Zhang Y, Hao Z, et al. Drude conductivity of Dirac fermions in graphene. Phys. Rev.B 2011;83.

[35] Zhao Y, Grischkowsky DR. 2-D terahertz metallic photonic crystals in parallel-plate waveguides. IEEE T Microw Theory 2007;55:656–63.

[36] Romaner L, Heimel G, Ambrosch Draxl C, Zojer E. The dielectric constant of self-assembled monolayers. Adv Funct Mater 2008;18:3999–4006.

[37] Alloway DM, Hofmann M, Smith DL, Gruhn NE, Graham AL, Colorado R, et al. Interface dipoles arising from self-assembled monolayers on gold: UV-photoemission studies of alkanethiols and partially fluorinated alkanethiols. J Phys Chem B 2003;107:11690–9.

[38] Sun Y, Xia X, Feng H, Yang H, Gu C, Wang L. Modulated terahertz responses of split ring resonators by nanometer thick liquid layers. Appl Phys Lett 2008;92:221101.

[39] Giovannetti G, Khomyakov P, Brocks G, Karpan V, Van den Brink J, Kelly P. Doping graphene with metal contacts. Phys Rev Lett 2008;101:026803.

[40] Nikolaenko AE, De Angelis F, Boden SA, Papasimakis N, Ashburn P, Di Fabrizio E, et al. Carbon nanotubes in a photonic metamaterial. Phys Rev Lett 2010;104:153902.

[41] Panoiu NC, Osgood R. Influence of the dispersive properties of metals on the transmission characteristics of left-handed materials. Phys Rev E 2003;68:016611.

[42] Driscoll T, Andreev GO, Basov DN, Palit S, Cho SY, Jokerst NM, et al. Tuned permeability in terahertz split-ring resonators for devices and sensors. Appl Phys Lett 2007;91:062511.

[43] Wu X, Quan B, Pan X, Xu X, Lu X, Gu C, et al. Alkanethiol-functionalized terahertz metamaterial as label-free, highly-sensitive and specific biosensor. Biosens Bioelectron 2013;42:626–31.

[44] Mori N, Ando T. Electron-optical-phonon interaction in single and double heterostructures. Phys Rev B 1989;40:6175.

[45] Fischetti MV, Neumayer DA, Cartier EA. Effective electron mobility in Si inversion layers in metal–oxide–semiconductor systems with a high-κ insulator: the role of remote phonon scattering. J Appl Phys 2001;90:4587–608.

[46] Fratini S, Guinea F. Substrate-limited electron dynamics in graphene. Phys Rev B 2008;77:195415.

[47] Kang YJ, Kang J, Chang K. Electronic structure of graphene and doping effect on SiO_2. Phys Rev B 2008;78:115404.

[48] Crowther Andrew C, Ghassaei Amanda, Jung Naeyoung, Jung Naeyoung, Brus LE. Strong charge-transfer doping of 1 to 10 layer graphene by NO_2. ACS Nano 2012;6:1865–75.

[49] Singh AK, Uddin MA, Tolson JT, Maire-Afeli H, Sbrockey N, Tompa GS, et al. Electrically tunable molecular doping of graphene. Appl Phys Lett 2013;102:043101.

[50] Kasry Amal, Kuroda Marcelo A, Martyna Glenn J, Tulevski George S. Chemical doping of large-area stacked graphene films for use as transparent conducting electrodes. ACS Nano 2010;4:3839–44.

[51] Hong G, Wu QH, Wang C, Ren J, Xu T, Zhang W, et al. Surface doping of nitrogen atoms on graphene via molecular precursor. Appl Phys Lett 2013;102:051610.

[52] Bae S, Kim H, Lee Y, Xu X, Park JS, Zheng Y, et al. Roll-to-roll production of 30-inch graphene films for transparent electrodes. Nat Nanotechnol 2010;5:574–8.